Supplementary Information

Experimental methods

SAM Preparation: Gold substrates were prepared by evaporating 5 nm Ti and 50 – 100 nm Au on Si <100> wafers and cleaving the wafers into pieces approximately 1 cm^2 in size. The MHA and MUA monolayers on gold surfaces were prepared by immersing gold substrates for 24 to 30 hours into 2 mM MHA or MUA solutions of 95% ethanol and 5% acetic acid.[1] After removal from the ethanolic solutions, the gold substrates were thoroughly rinsed with the corresponding pure solvent, 5% acetic acid in ethanol, and then dried by flow of nitrogen gas. SAMs were covered by DI water to eliminate potential oxidization and then instantly placed in the flow cell of the optical microscope.

Solution preparation: Ca^{2+} and CO_3^{2-} solutions were prepared from DI water and reagent grade $CaCl_2$ and $NaHCO_3$ for concentrations of: 10 mM, 18 mM, 20 mM, 21 mM, 22.5 mM, 24 mM, 25 mM, 26 mM, 27 mM, 28 mM, 29 mM, and 30 mM. Outside of this concentration range, we found that nucleation rates were either too fast or too slow to be successfully analyzed. The activities of Ca^{2+} and CO_3^{2-}, and supersaturation relative to calcite and ACC were calculated using MINTEQ[2] (Table S1). The equilibrium solubility products (K_{sp}) of calcite and ACC were based on the values of $10^{-8.48}$ and $10^{-6.393}$.[2,3]

Table S1

	$\{Ca^{2+}\}$	$\{CO_3^{2-}\}$	σ (calcite)	σ (ACC)
10 mM	4.45E-03	2.48E-05	3.506	-1.299
15 mM	5.84E-03	3.14E-05	4.014	-0.791
20 mM	7.04E-03	3.71E-05	4.368	-0.437
21 mM	7.26E-03	3.81E-05	4.425	-0.379
22 mM	7.48E-03	3.92E-05	4.483	-0.322
23 mM	7.69E-03	4.02E-05	4.536	-0.269
24 mM	7.90E-03	4.11E-05	4.58	-0.218
25 mM	8.11E-03	4.21E-05	4.635	-0.170
26 mM	8.31E-03	4.30E-05	4.683	-0.122
27 mM	8.51E-03	4.40E-05	4.727	-0.078
28mM	8.71E-03	4.49E-05	4.770	-0.034
29 mM	8.90E-03	4.58E-05	4.812	0.0069
30 mM	9.10E-03	4.67E-05	4.853	0.0483

Optical microscopy: A schematic image of the optical setup is illustrated in Figure S1. $CaCl_2$ and $NaHCO_3$ solutions were loaded into separate syringes of an automated syringe pump. $CaCl_2$ was first injected into the fluid cell before flowing through an equal mixture of $CaCl_2$ and $NaHCO_3$ solutions of equal concentrations in order to achieve better face-selective control.[4] We tested flow rates from 0.5 to 5 mL/min and found that the $CaCO_3$ nucleation rate increased as the flow rate increased from 0.5 to 2 mL/min, but did not change if the rate was increased further. Therefore, the flow rate was set to 2 mL/min, to yield nucleation rates independent of flow rate. This ensured that the nucleation was not limited by diffusion but was controlled by the nucleation reaction at the SAM surface. The tubing length was adjusted to ensure adequate mixing with little or no nucleation occurring prior to entering the fluid cell A tubing length of around 38 cm provided the highest rate of nucleation on the SAMs. The SAMs were placed upside down in the flow cell to prevent spurious nuclei from the solution from landing on the SAMs. $CaCO_3$ nucleation on the SAMs was imaged *in situ* using an inverted optical microscope in an area of 0.65 - 0.49 mm^2. Because the critical radius of a $CaCO_3$ nucleus was expected to be well below the resolution limit of the optical system, the nuclei were too small to be observed by the optical microscope at the instant of formation, so we assumed that each observed crystal developed from one nucleus. This assumption was reasonable because the observed nucleation density was so low that the average distance between neighboring nuclei was much greater than the size at which the nuclei became visible. The observed linear dependence between number of nuclei and time after the onset of nucleation validates this assumption.

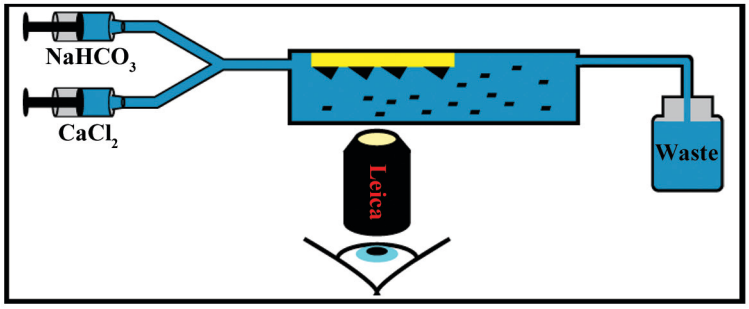

Fig. S1 – Schematic of experimental set-up for measuring nucleation rates. The SAM is suspended upside-down in a flow-through cell and imaged using an inverted optical microscope to measure nucleation rates as supersaturated calcium carbonate solutions are continuously pumped through the cell to maintain constant supersaturation.

Molecular dynamics simulations: Molecular dynamics simulations were performed using the DL_POLY classic code (version 1.4)[5] with a time step of 1 fs. Simulations were all performed using the NVT hoover thermostat with a relaxation time of 0.02 ps at a temperature of 300 K. The configurations of the SAMs were those used in previous simulations,[6] with a total of 48 chains arranged in a hexagonal layout in a box measuring 33.2 Angstrom x 28.8 Angstrom in the plane of the monolayer. The SAM chains were 16-mercaptohexadecanoic acid (even) and 15-mercaptopentadecanoic acid (odd). For all the simulations described the SAMs were fully ionised and therefore 24 Ca^{2+} cations were introduced to the system to maintain charge neutrality. A total of 480 water molecules were placed above the SAM surface for simulations of the SAM-water interface. The simulations with $CaCO_3$ used the final geometries from previous metadynamics crystallization simulations.[7] In these simulations the 480 water molecules were placed in contact with the exposed $CaCO_3$ surface not at the interface with the SAM. The sulfur atom at the base of each chain was fixed during the simulation but all other atoms were allowed full mobility. The united atom model from the CHARMM forcefield[8,9] was used to described the SAM chains with the head groups modeled explicitly. Water molecules were modeled with the TIP3P model[10] and the $CaCO_3$ ions were modeled with the Pavese forcefield.[11.12] Cross-term interactions were derived via the method of Schroder et al[13] as demonstrated for $CaCO_3$.[14] Simulations were run until the 250 ps block energies showed a variation of less than 20 kJ/mol (typically 5 ns) from the simulation average and the energies reported were collected over the final 1 ns.

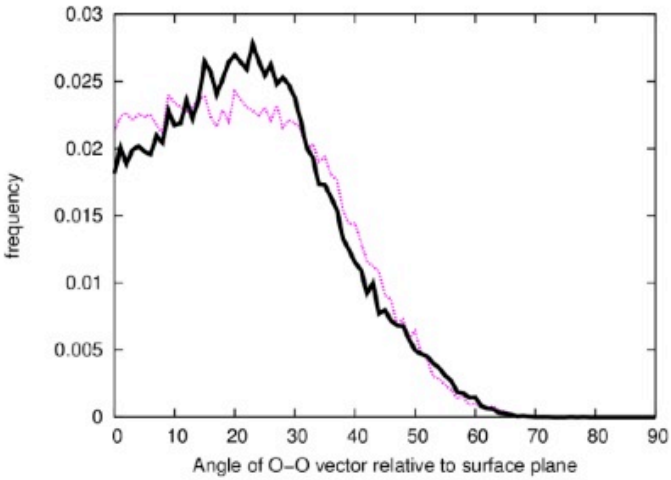

Fig. S2 - Angular distribution of the O-O vector with respect to the surface plane of the SAM for the even (dashed magenta) and odd (solid black) SAMs in contact with water.

It is not possible to directly extract free energies from molecular dynamics simulations as entropy is related directly to the partition function and requires special methods for its calculation. Therefore the energies returned are configurational energies (since the simulation is performed within an NVT ensemble). However, the difference between these values for odd and

even configurations would be expected to be similar to the difference between the experimental free energies since the configurations of the odd and even SAMs are much alike and so the vibrational component of the simulations will be nearly identical in both odd and even SAMs and therefore tend to cancel out. Moreover, since the process of determining the interfacial energies requires finding the differences between two simulations the vibrational contributions should cancel even for the individual values. Absolute crystal-film (acf) and film-solution (afs) interfacial energies cannot be calculated from simulation as there is no suitable reference state for the isolated film. Calculation of the difference between acf and afs (i.e. acf-afs) is possible (since the reference state of the isolated film cancels out) by performing multiple simulations of the film-solution, film-crystal and crystal-solution interfaces and determining the differences between them which can then be used within equation S1 to determine the interfacial energy required. See reference 15 for a detailed discussion of the simulations necessary to calculate this value.

Raman analysis: Samples were quenched in the optical cell by changing the flow from calcium carbonate solution to ethanol, as described previously for quenching of calcium phosphate samples.[16] Precipitates collected right after quenching exhibited Raman patterns characteristic of calcite with peaks at 154 cm^{-1}, 284 cm^{-1},710 cm^{-1} and 1084 cm^{-1} .[17,18] However, the distinctive broad peak of ACC at 150-300 cm^{-1} [19,20] did not occur in any of the patterns. Since the volumes of the smallest particles are at the lower detection limit of micro-Raman, the peaks are not as sharp as the ones from the other two morphologies. (The 520 cm^{-1} peak is that of Si from silicon wafer.)

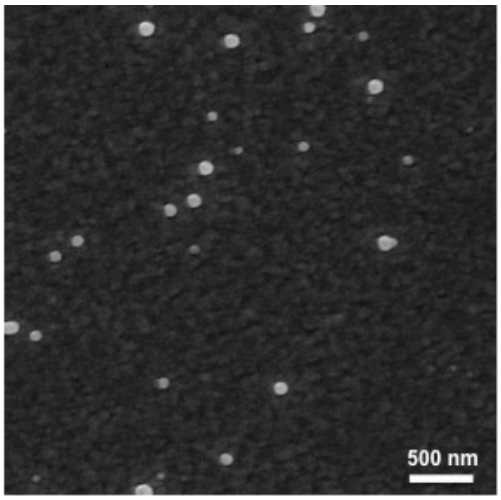

Fig. S3 – SEM image of 23 mM sample on MUA film recovered from optical flow cell showing sporadic occurrence of sub-100 nm particles. Mottled background reflects roughness of sputtered Au films used as substrates for SAMs.

Atomic Force Microscopy: *In-situ* atomic force microscopy was measured by using an AFM liquid cell with either contact or tapping mode AFM (Digital Instruments J scanner, Nanoscope IIIa and V controllers, Veeco Metrology, Inc., Santa Barbara, CA) using hybrid probes consisting of silicon tips on silicon nitride cantilevers (Sharp Nitride Lever, k = 0.35 N/m, tip radius < 10 nm; Bruker AFM

probes, and Hydra, k = 0.035 N/m, tip radius < 10 nm; AppNano.). The tapping mode was adopted in these experiments while applying a loading force less than 50 pN using optimized feedback and set-point parameters for stable imaging conditions. About 100 µL of growth solutions were injected into the sealed liquid cell and the image was captured immediately after the solution injection. Measurements were made by mixing equal $CaCl_2$ and $NaHCO_3$ with the final concentrations of 13 mM and 25 mM on the surface of hydroxyl-terminated SAMs and between 20 mM and 40 mM on the surface of carboxyl-terminated SAMs. SAM preparation followed the same procedure as used in the optical experiments, using MUO and MHA for hydroxyl-and carboxyl-SAMs, respectively. In order to increase the image stability and nuclei density, *in-situ* AFM experiments were also carried out by diffusion method with ammonium carbonate diffusing into 50 mM $CaCl_2$ on the surface of OH terminated SAMs or mica. No obvious differences were observed between these two methods or substrates. The first particle was observed within 1 min for mixing method and up to 30 min for diffusion method, however, all of these particles were dissolved within 5 min when the rhombohedral crystal formed separately.

TEM analysis: TEM samples used the same solution preparation method described for the AFM analysis. Subsequent to filtering the solutions, equal amounts were pipetted into a 1 mL centrifuge tube and spun at 6000 rpm in a Galaxy Ministar centrifuge (VWR) for 1-2 minutes, depending on concentration. The supernatant liquid was quickly removed and replaced with pure ethanol and the sample was centrifuged for another minute. This was repeated three times. After the final rinse, ethanol was used to wash any solid off the centrifuge tube walls and suspend the material in solution. A drop of this solution was placed on a TEM grid which was immediately placed into vacuum and pumped into the millitorr range. The TEM grid was then removed from vacuum, secured onto a TEM stage, and inserted into a JEOL 2100F operating at 200kV for analysis.

Carbonate diffusion optical experiments: Carbonate diffusion experiments were conducted by placing OH and COOH SAM substrates in a covered 100 mm diameter petri dish, elevating the substrate to just below the inner surface of the lid. A small droplet of a few to a few tens of microliters of $CaCl_2$ solution, 10-50 mM, was placed on the substrate, and a 20 mm diameter

dish containing less than a gram of $(NH_4)_2CO_3$ was placed nearby the substrate in the larger dish. The lid was then replaced on the larger dish and the dish was moved such that the substrate was in the focal plane of a light microscope and the first image was collected, establishing a zero time point. This time point was five to ten seconds after closing the dish. Sequential images were captured every five to ten seconds following the zero time point.

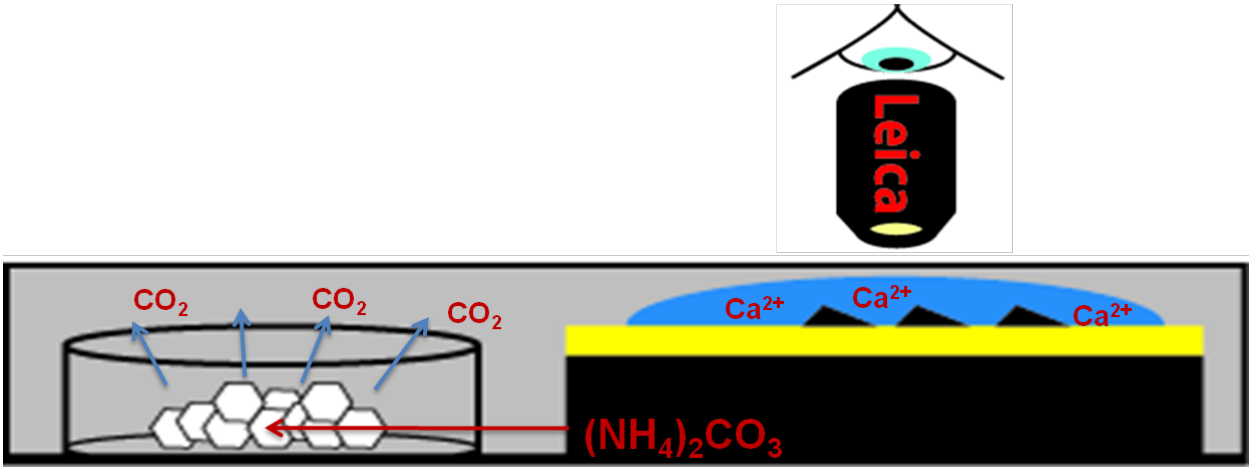

Fig. S4 – Schematic showing set-up for optical experiments to observe calcium carbonate nucleation during diffusion of carbonate into a $CaCl_2$ solution. The upward-facing SAM is covered with a droplet of $CaCl_2$ solution in a closed optically transparent container. $(NH_4)_2CO_3$ is placed in an open dish near the droplet and nucleation is observed through an optical microscope.

Dependence of nucleation rate on supersaturation: In classical nucleation theory (CNT), the free energy change upon nucleation is given by:[16]

$$\Delta g = -\frac{V}{\Omega}\mathbf{k}T\sigma + A_b(\alpha_{cs} - \alpha_{fs}) + A_s\alpha_{cf} \quad \text{(S1)}$$

where V is the volume of the nucleus, Ω is the molecular volume of the growth unit — equal to 6.13E-23 cm^3 for calcite[21] — $\mathbf{k}$ is Boltzmann's constant, T is the absolute temperature, σ is the supersaturation, A_b is the area of the base in contact with the film, A_s is the area of the surface in contact with the solution, and α_{cf}, α_{fs} and α_{cs} are the interfacial energies of the crystal-fluid, fluid-substrate and crystal-substrate interfaces. The thermodynamic barrier is given by the maximum in Δg, which occurs at:

$$\Delta g_c = \frac{f\alpha^3\Omega^2}{(\mathbf{k}T\sigma)^2} \quad \text{with} \quad \alpha = \alpha_{cf} - h(\alpha_{fs} - \alpha_{cs}) \quad \text{(S2)}$$

and the corresponding nucleation rate is given by:

$$J = Ae^{-E_A/kT}e^{-\Delta g_c/kT} \text{ or } \ln(J) = A' - \frac{f\alpha^3\Omega^2}{(\mathbf{k}\boldsymbol{T})^3}\left(\frac{1}{\sigma^2}\right) \text{ with } A' = ln(Ae^{-\frac{E_A}{kT}}) \quad \text{(S3)}$$

where A is a pre-factor that is independent of σ, and E_A is an effective activation barrier that captures the kinetic barriers to reactions such as desolvation of solute ions, attachment to the forming nucleus and structural rearrangements. Here both f and h are numbers that depend on the aspect ratio of the nucleus. For nucleation of a calcite rhombohedron on the (012) plane, analysis of the volume and surface areas leads to f = 19.71 and h = 0.525. However, for a large range of nucleation planes, these numbers are nearly identical, varying by no more than about 10%. Because the interfacial energy is raised to the third power in the free energy barrier, these small variations in f have negligible effect (<2.5%) on the values of α extracted from the nucleation rate data.

The interfacial free energy can be generalized to an excess free energy, Δg_{ex}. In this regard, the change in free energy associated with formation of a solute particle is given by:

$$\Delta g = \frac{dg}{dn}\Delta n + \Delta g_{ex} \quad \text{(S4)}$$

In CNT Δg_{ex} is given by the interfacial energy times the surface area of the nucleus, which is assumed to be constant. Consequently, Δg_{ex} scales with the square of the particle size, i.e., $\Delta g_{ex}/A_s = \alpha$ = constant. Two factors that can have a further and significant impact on the nucleation barrier are a more complex size dependence and the existence of local minima in Δg_{ex} vs. size.

The effect of size dependence can easily be incorporated. For example, if the size dependence is given by an exponential rise from a minimum value, then $\Delta g_{ex} = \alpha_\infty A_s\{1\text{-}exp[-(L\text{-}L_0)/L_\infty]\}$., where L is the edge length of the rhombohedron, L_0 is the value of L at which Δg_{ex} decreases to zero, and is L_∞ the value of L at which Δg_{ex} reaches 1 – exp[-(1-L_0/L_∞) of its bulk value. When the critical size is of the order of or less than the dimensions at which the dependence of the excess free energy on size becomes significant, the consequence of is a reduction in the energy penalty associated with creating the critical nucleus. The impact of this effect is shown in Figure 2B.

The effect of clusters can also be incorporated into Eqn S1 by writing:

$$\Delta g = -\frac{V}{\Omega}\mathbf{k}T\sigma + A_b(\alpha_{cs} - \alpha_{fs}) + A_s\alpha_{cf} - \frac{V}{V_{cl}}\Delta g_{ex} \quad \text{(S5)}$$

where V_{cl} and Δg_{Ex} are the volume and excess free energy of a cluster above that of the free ions. For homogeneous nucleation of rhombohedral calcite of edge length L from spherical clusters of radius r_{cL}, $\frac{V}{V_{Cl}} = 0.978 \bullet L^3/4\pi r_{Cl}^3$ giving:

$$\Delta g = -\frac{0.978L^3}{\Omega}\mathbf{k}T\sigma + 6 \bullet 0.978\mathrm{L}^2\alpha_{cf} - \frac{0.978 \bullet L^3}{\frac{4}{3}\pi r_{cl}^3}\Delta g_{ex} \quad \text{(S6)}$$

When the clusters lie in a local minimum, $\Delta g_{ex} > 0$ (Figure 2D, solid green line). Therefore, because the clusters lie higher in free energy than the ions, aggregating them to form a critical nucleus carries less of an energy penalty. On the other hand, if the clusters lie in a global minimum, i.e., they are lower in energy than the free ions, $\Delta g_{ex} < 0$ (Figure 2D, dashed green line) and there is an added energy penalty associated with nucleation through their aggregation. The impact of cluster aggregation for positive Δg_{ex} is illustrated in Figure 2C.

Beyond inducing changes in the magnitude of the barrier, the second effect of these features in the free energy landscape is that the relationship between the barrier (or rate) and the supersaturation deviates from the simple α^3/σ^2 dependence seen in Eqn. S2 and S3. Even in the case of a simple size dependence, such as the exponential rise described above, the resulting relationship is complex. In the case of cluster aggregation in an otherwise flat landscape, if we write $\Delta g_{ex} = 4\pi r_{cl}^2\alpha_{cl}$, where α_{cl} is the effective interfacial energy of a cluster, then in Eqn. S3 σ is simply replaced by:

$$\sigma' = \sigma + \frac{3\Omega\alpha_{cl}}{r_{cl}\mathbf{k}T} \quad \text{(S7)}$$

In the case where the minimum is global, there is a stable population of clusters with a narrow size distribution and the plus sign in Eqn. S7 is replaced with a minus sign. For $r_{cl} \geq 0.5$ nm, $\alpha_{cl} \leq 0.5\alpha$ and $\sigma \geq 4.5$, Eqn. S7 gives $\frac{\sigma' - \sigma}{\sigma} < 0.1$. Consequently, for the range of concentrations examined in this study, deviations from α^3/σ^2 due to cluster aggregation are unlikely to be observed.

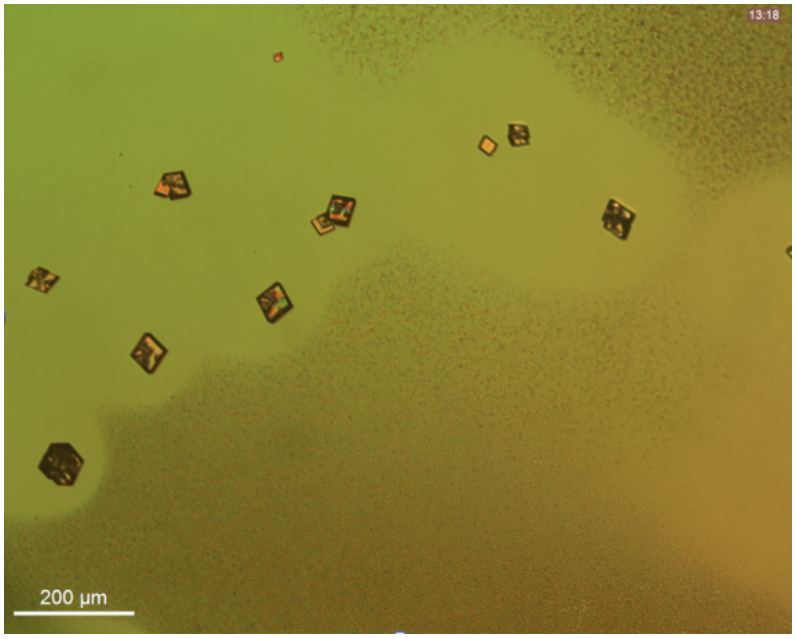

Movie S1 – Formation of ACC film on OH-terminated SAM followed by nucleation of calcite rhombs, which grow as the ACC film dissolves.

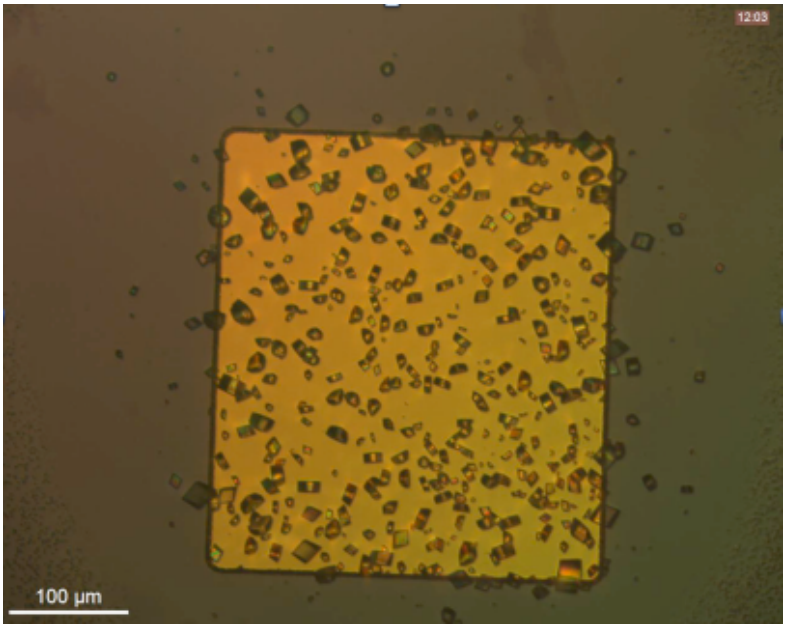

Movie S2 – Apparent direct formation of calcite on carboxyl-terminated SAM (MHA) under same conditions used for **Movie S1**.

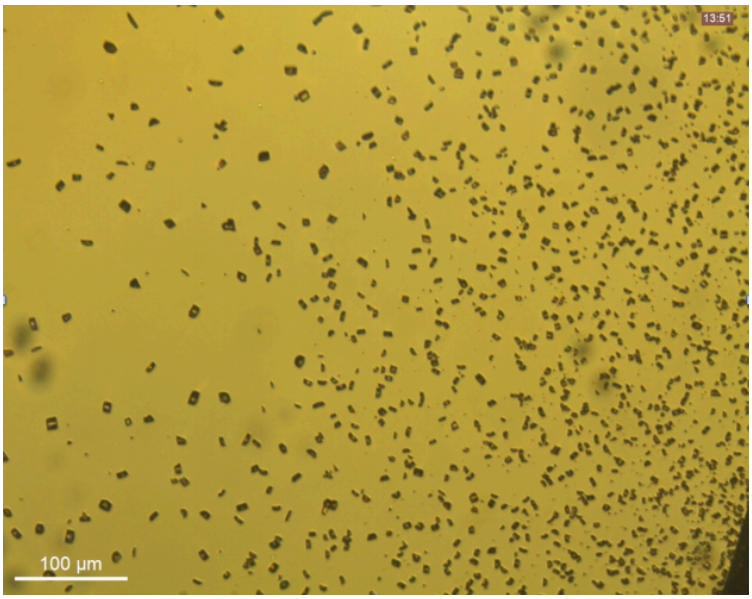

Movie S3 – Apparent direct formation of calcite on carboxyl-terminated SAM (MHA) under same conditions used for **Movie S2.** With the large SAM area, no ACC forms because the formation of calcite across the entire surface prevents the supersaturation from reaching the required level.

References

1. Lee, J.R.I., et al., *J. Am. Chem. Soc.*, 2007. **129**, 10370-10381.
2. Allison, J.D., D.S. Brown, and K.J. Novo-Gradac, *MINTEQA2/PRODEFA2, a geochemical assessment model for environmental systems: Version 3. 0 user's manual*, in *US Environmental Protection Agency, Athens, GA*. 1991. p. 117
3. Brecevic, L. and A.E. Nielsen, *J. Cryst. Growth*, 1989, **98**, 504-510.
4. Aizenberg, J., A.J. Black, and G.M. Whitesides, *J. Am. Chem. Soc.*, 1999, **121**, 4500-4509.
5 Smith, W., *J. Mol. Graphics*, 1996, **14**, 136-141.
6 Duffy, D.M., *Langmuir*, **20**, 2004, 7637-7642.
7 Quigley, D., *J. Chem. Phys*., 2009, **131**, 094703.
8 Moller, M.A., *J. Chem. Phys.*, 1991, **94**, 8390-8401.
9 MacKerell, A., *J. Phys. Chem.*, 1998, **B 102**, 3586-3616.
10 Jorgensen, W.L., *J. Chem. Phys*., 1983, **79**, 926-935.
11 Pavese, A., *Phys. Chem. Miner*., 1992, **19**, 80-87.
12 Pavese, A., *Phys. Chem. Miner*., 1992, **23**, 89-93.
13 Schroder, K.-P., *Chem. Phys. Lett*., 1992, **188**, 320-325.
14 Freeman, C.L., *J. Phys. Chem.*, 2007, **C 111**, 11943-11951.
15 Duffy, D.M., *Langmuir*, 2004, **20**, 7630-7636.
16. De Yoreo, J.J. and P.G. Vekilov, *Reviews in Mineralogy and Geochemistry*, 2003, **54**, 57-93.
17. Rull Perez, F., and Martinez-Frias, J., *J. Raman Spectroscopy*, 2003, **34**, 367-370.
18. Urmos, J., Sharma, S.K., and Mackenzie, F.T., *Amer. Min*., 1991, **76**, 641-646.
19. Addadi, L., Raz, S., and Weiner, S., Adv. Mater., 2003, **15**, 959-970.
20. Raz, S., Testeniere, O., Hecker, A., Weiner, S., and Luquet, G. *Biol Bull.*, 2002, **203**, 269-274.
21. Davis, K.J., Dove, P.M. and De Yoreo, J.J., *Science,* 2000, **290,** 1134-1137.